OCT Minimum Intensity as a Predictor of Geographic Atrophy Enlargement

Paul F. Stetson,[1] Zohar Yehoshua,[2] Carlos Alexandre A. Garcia Filho,[2] Renata Portella Nunes,[2] Giovanni Gregori,[2] and Philip J. Rosenfeld[2]

[1]Research and Development, Carl Zeiss Meditec, Inc., Dublin, California
[2]Bascom Palmer Eye Institute, University of Miami Miller School of Medicine, Miami, Florida

Correspondence: Paul F. Stetson, Carl Zeiss Meditec, Inc., 5160 Hacienda Drive, Dublin, CA 94568-7562; paul.stetson@zeiss.com.

Submitted: September 4, 2013
Accepted: December 17, 2013

Citation: Stetson PF, Yehoshua Z, Garcia Filho CAA, Portella Nunes R, Gregori G, Rosenfeld PJ. OCT minimum intensity as a predictor of geographic atrophy enlargement. *Invest Ophthalmol Vis Sci*. 2014;55:792–800. DOI:10.1167/iovs.13-13199

Purpose. We determined whether the minimum intensity (MI) of the optical coherence tomography (OCT) A-scans within the retina can predict locations of growth at the margin of geographic atrophy (GA) and the growth rate outside the margin.

Methods. The OCT scans were analyzed at baseline and 52 weeks. Expert graders manually segmented OCT images of GA. The 52-week follow-up scans were registered to the baseline scan coordinates for comparison. The OCT MI values were studied within a 180-μm margin around the boundary of GA at baseline. Baseline MI values were compared in areas of progression and nonprogression of the GA, and sensitivity and specificity were assessed for prediction of growth at the margin. Average MI values in the margins were compared to overall growth rates to evaluate the prediction of growth outside the margins.

Results. A statistically significant increase in MI ($P < 0.05$) was seen in areas of growth in 21/24 cases (88%), and 22/24 cases (92%) when the foveal subfield was excluded. Locations of growth within the margins at 52 weeks were predicted with 61% sensitivity and 61% specificity. The MI values correlated significantly with overall growth rate, and high and low growth rate subjects were identified with 80% sensitivity and 64% specificity.

Conclusions. The MI may be increased at the margins of GA lesions before enlargement, which may indicate disruption or atrophy of the photoreceptors in these areas before GA becomes apparent. Increased MI may help predict areas of enlargement of GA, and may relate to overall growth rate and be a useful screening tool for GA. (ClinicalTrials.gov number, NCT00935883.)

Keywords: geographic atrophy, GA, AMD, image processing, macula

The appearance of geographic atrophy (GA) related to age-related macular degeneration (AMD) is characterized by a loss of photoreceptors, retinal pigment epithelium, and choriocapillaris, but it is not known whether the loss of one of these features consistently precedes the others. Typically, GA lesions first will appear parafoveally, proceed to encircle the fovea to a large extent, and then progress into the fovea.[1,2] Since the area of GA is associated with a scotoma corresponding to the location of the atrophy, the ability to identify the location of future progression of GA may help determine the risk of central vision loss and help assess whether potential therapies can prevent or slow the progression of atrophy. Identifying anatomic changes that precede the expansion of GA also may be useful in identifying lesions that grow faster than others and help in stratifying subjects with higher growth rates for studies evaluating new treatments for GA.

Spectral domain optical coherence tomography (OCT) can be used to image and measure GA.[3,4] Several studies have used OCT to describe a wide spectrum of morphologic alterations that appear within the atrophic area, as well as within the surrounding retinal tissue.[5–9] A common finding within the atrophic lesions is the absence of the ONL, as well as OCT bands corresponding to anatomic layers, including the external limiting membrane, inner segment/outer segment (IS/OS) junction, and the RPE/Bruch's membrane complex.[8] Schmitz-Valckenberg et al.[10] compared the fundus autofluorescence (FAF) and OCT appearance of eyes with GA, and showed that the mean length of an atrophic lesion measured on the FAF image had the closest agreement with the appearance of choroidal hyperreflectivity on the OCT B-scan, and the reduction of the FAF signal seen from GA is correlated spatially with the abrupt transition on the OCT B-scan from a hyporeflective choroid to a hyperreflective choroid. This increased penetration of light below Bruch's membrane presumably is due to the loss of the RPE and choriocapillaris.[4,7] Sayegh et al.[11] also showed that the area of choroidal signal enhancement on the OCT B-scans correlated well with the hypofluorescent area measured on FAF.[4]

As seen in OCT B-scan images, the enlargement of GA is characterized by the progressive loss of the outer hyperreflective bands corresponding with the RPE/Bruch's membrane complex and by thinning of the ONL with subsequent approach of the outer plexiform layer toward Bruch's membrane. There appears to be a high degree of variability in how the borders of GA change, as seen from OCT B-scans, both when comparing different locations along the border of GA in a given eye and across different patients.[9]

Spectral domain OCT imaging also can provide en face images of GA that complement the B-scan cross-sectional images. These images are generated by summing the signal of each of the A-scans and viewing their relative values en face.[7,12,13] In this en face view, the GA appears as a bright area

due to the increased penetration of light into the highly reflective choroid in areas where atrophy has occurred in the macula. This imaging of GA correlates well with the GA appreciated on clinical examination, fundus photography, and autofluorescence imaging.[3,4] This current study uses a relatively new approach for imaging GA, introduced in the Cirrus Advanced RPE Analysis, known as the Sub-RPE Slab, which creates the en face image only from the light reflected from beneath the RPE. By using only the light that penetrates into the choroid, the Sub-RPE Slab has higher contrast at the borders of GA and the GA appears more distinct.[14]

The appearance and progression of GA has been studied extensively using reflectance fundus photography,[2,15] FAF,[16] and OCT.[3] These imaging strategies have provided some clues regarding the appearance and progression of GA. Reflectance imaging has identified drusen, hyperpigmentation, and reticular pseudodrusen as risk factors for the appearance and progression of GA.[17–21] Autofluorescence imaging has identified different hyperautofluorescence patterns of the RPE, and these patterns have been associated with different growth characteristics of GA.[6,22–24] The OCT has identified subretinal drusenoid deposits, and abnormalities of the RPE and photoreceptors at the margins of GA that may be associated with the expansion of GA.[6–10,25] However, none of these imaging strategies have predicted reliably the specific areas in the macula where GA is likely to appear or predicted the specific pattern of GA growth over a given interval of time. To help predict where GA is likely to appear and grow, investigators have relied on functional testing of the retina.[17]

The loss of photoreceptors away from the edge of GA has been identified histopathologically, and dysfunctional photoreceptors have been detected away from the edge of GA using electrophysiology and microperimetry threshold testing.[17] Microperimetry has detected photoreceptor abnormalities even before GA develops, and this strategy also can predict the area where existing GA likely will progress.[26–32] These histopathologic, electrophysiologic, and microperimetric findings in eyes with GA, along with the early visual function deficits and symptoms observed in patients even before GA develops,[33] suggest that photoreceptor dysfunction precedes the appearance and progression of GA in some eyes.

The structural disruption of the photoreceptors distant from the margin of GA lesions also may be observed using OCT. Nunes et al.[34] describe cases in the same study dataset used here, where disruption of the IS/OS boundary was found to extend at varying distances from the margins of the GA and was related to the subsequent area of progression.

In this study, we used a different analysis of the OCT data to visualize photoreceptor disruption. We examined the lowest image intensity from each A-scan within the retina, the minimum intensity (MI). In normal areas of retina, the darkest part of each OCT A-scan nearly always lies within the outer nuclear layer (ONL) or Henle fiber layer (HFL), which contain photoreceptor cell bodies and axons. In the presence of certain pathologies, though, the reflectivity of these layers may be altered (Dupas B, et al. *IOVS* 2010;51:ARVO E-Abstract 924). The reflectivity of these normally dark layers often becomes slightly elevated in the vicinity of focal pathology. Changes in the MI previously were found often to represent abnormalities in the reflectivity and integrity of the ONL and HFL (Soudry S, et al. *IOVS* 2011;52:ARVO E-Abstract 4799). In previous work, we also found that MI was increased significantly in areas of future growth at the margin of GA (Stetson PF, et al. *IOVS* 2012;53:ARVO E-Abstract 2047). This study seeks to confirm those findings at the 52-week follow-up, and to examine whether the elevated reflectivity of those layers might predict the appearance and progression of GA, locally and globally.

Methods

Subjects and Acquisition

Patients with GA measuring from 1.25 to 18 mm^2 were enrolled prospectively. To be enrolled in this study, patients had to have at least one eye with GA measuring from 1.25 to 18 mm^2, with unifocal or multifocal GA lesions contained within a 6×6 mm area centered on the fovea. Enrollment also required a visual acuity of 20/63 or better (60 letters) as measured using a standard visual acuity testing protocol with the Early Treatment Diabetic Retinopathy Study chart at 4 m. Patients were excluded from the study if the study eye demonstrated areas of peripapillary atrophy communicating with the area of macular atrophy. Patients also were excluded if the study eye presented any sign or history of choroidal neovascularization, or any confounding ocular conditions, such as retinal detachment, severe nonproliferative or proliferative diabetic retinopathy, retinal vascular occlusion, macular edema, evidence of inherited retinal degeneration, and a history of pars plana vitrectomy. The study was approved by the institutional review board of the University of Miami Miller School of Medicine and conducted in accordance with the tenets of the Declaration of Helsinki. Each patient gave consent after being informed about the nature and possible consequences of the study.

The OCT imaging was acquired at baseline and 52 weeks, using a Cirrus HD-OCT (Carl Zeiss Meditec, Inc., Dublin, CA), a spectral domain OCT device with an axial resolution of 5 μm and a scanning rate of 27,000 A-scans per second. Data also were acquired at 13 and 26 weeks, but those time points were not used for this study. All scans were performed by a single research technician on a single instrument, who assessed the quality of the scan during its acquisition. All scans were performed after dilation of the patient's pupil. The 200×200 scan pattern was used, covering a 6×6 mm area centered roughly on the fovea with A-scans separated by 30 μm vertically and horizontally. Attempts were made to obtain five good scans for each eye in each session; however, low-quality scans with signal strength less than 7, and scans with severe motion artifacts were discarded and repeated whenever possible. All measurements were made from a single scan with good signal strength and without motion artifacts.

Data Analysis

Segmentation of GA From Sub-RPE OCT Projection Images. Prototype algorithms used for the Cirrus HD-OCT were used to segment the inner limiting membrane (ILM) and RPE, and to perform a robust polynomial fit to the RPE segmentation. The GA was visualized using a Sub-RPE Slab, developed for the Cirrus Advanced RPE Analysis, formed by axially projecting the OCT image data from a region below the robust RPE Fit (Fig. 1). The region extends from 65 to 400 μm below the RPE Fit. Image processing was used to reduce noise and suppress the appearance of the choroidal vasculature. This shows the area of GA by the presence of areas of increased illumination below the RPE[14] (Lee BW, et al. *IOVS* 2011;52:ARVO E-Abstract 142).

The Sub-RPE Slab images were exported as a 200×200–pixel bitmap file to a CintiQ WACOM digitizing tablet (WACOM Corp., Vancouver, WA), and two expert graders manually drew the boundaries of the GA (Fig. 2). Comparing these two results, a consensus image was generated. In the cases in which the two graders could not reach an agreement on the outlines of the GA, a third senior grader (PJR) outlined the lesion and this was used for the analysis. The segmentation of each lesion was performed independently for the baseline and follow-up scans.

Investigative Ophthalmology & Visual Science

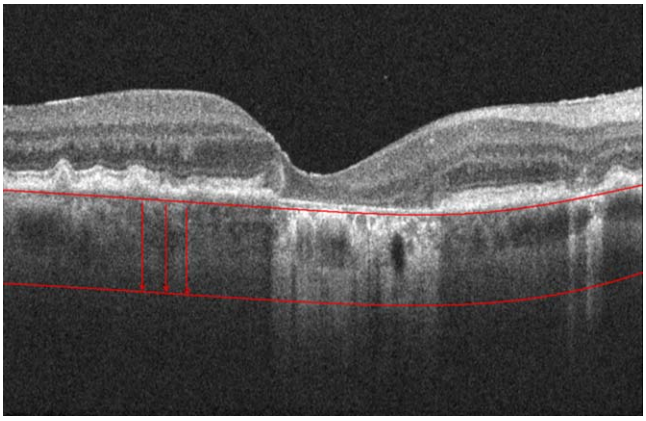

FIGURE 1. Subretinal pigment epithelium slab image. Axial integration highlights areas of illumination below the RPE.

Pixel areas were converted to square millimeters using the same fixed ratio established by the OCT instrument (36 mm^2/40,000 pixels). The growth rate of GA was measured using the square root transformation strategy described by Yehoshua et al.,[3] which has a lower dependency on lesion size than simply measuring the change in lesion area.

After segmentation, the results from the 52-week scans were mapped into the coordinates of the baseline scan using rigid transformation. The transformed results were reviewed to ensure that no misregistration of more than 100 μm occurred within 250 μm of the GA lesions.

Construction of the MI Image. The MI projection is a noninvasive en face imaging technique developed for OCT by Carl Zeiss Meditec, Inc.[35] The principle of the technique is to find the minimum of the speckle-reduced image along each A-scan between the ILM and RPE. Previous works on medical image processing have described the general principles of the MI projection.[36–38] In our study, the OCT scan first was segmented using the ILM and RPE algorithms used in the Cirrus system. The images were smoothed slightly to reduce the variation due to speckle. Each A-scan then was analyzed to find the darkest pixel between the ILM and RPE boundaries for that location. These darkest pixels from each A-scan in the 3-D image volume then were collected into a two-dimensional en face image called a Minimum-Intensity Projection (Fig. 3). Since this image originally consists of mostly dim pixels, the brightness and contrast are increased, and an estimate of variation in illumination is applied to reduce the effects of shadowing from opacities overlying the retina.

If an intraretinal or subretinal cyst contains no blood or other scattering material, the fluid reflectivity will be much lower than that of the surrounding tissue, and it will appear as a dark spot in the MI image. In normal areas of retina, the MI lies within the ONL/HFL nearly all of the time, and it appears gray in the MI image (Fig. 3). In the presence of certain pathologies, though, the reflectivity of the ONL/HFL may be increased. This can be observed in the OCT B-scans, and the increased MI generally becomes quite apparent in the en face visualization of the MI data as a lighter region than the surrounding gray background.

Statistical Analysis of the MI Values at the Margin of GA. The MI values were studied within a margin of 180 μm around the boundary of GA in the baseline scans (Figs. 4, 5). This margin width was chosen to give comparable numbers of pixels with progression and nonprogression, not necessarily for a particular case, but for the full set of cases. The 180-μm margin was not completely covered by GA at 52 weeks in any of the cases. Because smoothing of adjacent pixels was applied

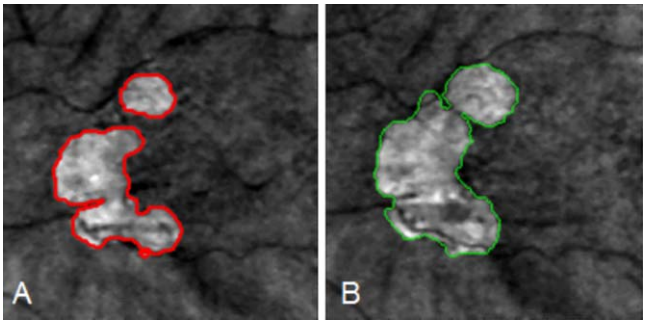

FIGURE 2. Manual segmentation of subretinal pigment epithelium slab images. (**A**) Image derived from baseline OCT scan. (**B**) Image derived from OCT scan performed after 52 weeks.

to the MI image, every second sample in the vertical and horizontal directions was excluded from the analysis to eliminate that smoothing as a source of correlation between sample points.

Analyzing each eye separately, MI values in areas with progression of GA over the 52-week follow-up period were compared using a 1-sided *t*-test (ttest2, MATLAB; Mathworks, Natick, MA) with MI values from areas that did not progress, yielding for each eye a *P* value that indicated the significance of increase in MI for the areas that later progressed to GA. Since the fovea often was observed to exhibit a low MI even in areas of GA, a second analysis was performed, in which data within 500 μm of the foveal center were excluded. For this step, foveas were located using the fovea finding algorithm employed by the Cirrus system.[39,40]

Since image intensity varies from scan to scan, comparison of MI values among different scans requires the comparison to be gauged relative to the values within each scan. The relationship in MI between the lesions and their surroundings is fairly consistent, so for these purposes the value of the MI at each pixel was assessed relative to the values inside and outside of the boundaries of the GA lesions for each case:

$$MI_{\text{relative}} = (MI - M_{\text{outside}})/(M_{\text{inside}} - M_{\text{outside}})$$

where M_{inside} and M_{outside} represent the mean values of MI observed inside and outside the boundaries of the GA lesions for the MI en face image from that case, with the boundaries of the GA being determined from the sub-RPE slab en face image from that same OCT scan.

To assess the ability to predict growth at a specific location in the margin by thresholding the MI image, a receiver operating characteristic (ROC) analysis was performed, analyzing locations of progression and nonprogression with their values of MI_{relative}. Because the MI often is decreased at the fovea, this analysis also was repeated with the 1-mm diameter circle around the foveal center excluded.

To assess the ability to predict the rate of growth outside the margin, the mean value of MI_{relative} within the 180-μm margin of the GA lesions was calculated, and these mean values for all the subjects were correlated with the observed 52-week changes in the square root of the lesion area. This square root–area growth rate has been shown previously to be less sensitive than the area growth rate to differences in baseline lesion area.[3] To assess the ability to distinguish between subjects with high and low growth rates, the subjects also were separated into high- and low-MI groups, based on whether the mean MI_{relative} within the 180-μm margin was greater or lower than 0.5, in other words, based on whether the mean MI at the margin was closer to that of the GA lesions or their surroundings. We then calculated the sensitivity and specificity

Investigative Ophthalmology & Visual Science

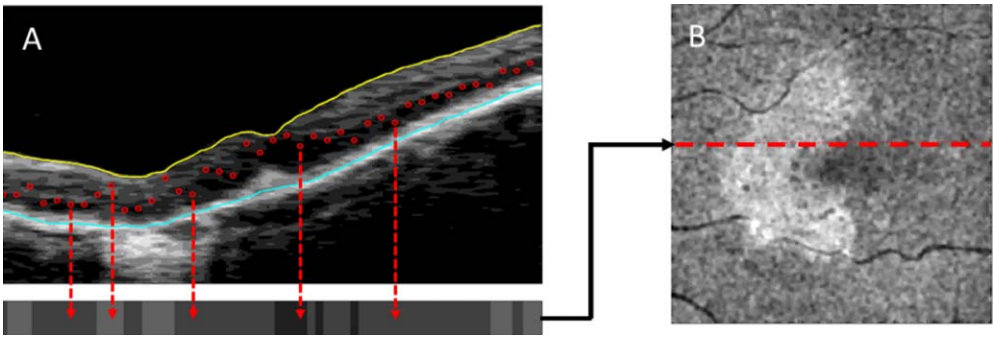

FIGURE 3. Construction of the MI image. (**A**) The same baseline OCT scan that was used for the subretinal pigment epithelium slab in Figure 2A was used to identify minima (*red circles*) from each speckle-reduced B-scan. (**B**) The minimum intensities were assembled into an en face image. Contrast of the en face image was enhanced.

of whether the high- and low-MI groups exhibited above- and below-average growth rates, respectively. The growth-rate analyses also were performed with and without data from the 1-mm diameter foveal circle.

A prototype segmentation was applied to the images to identify areas of increased MI. This algorithm approximates the histogram of the image grayscale levels as that of the sum of two Gaussian distributions, then defines a grayscale threshold between the peaks of those two Gaussian distributions. After the MI image was thresholded, patches smaller than a circle of radius 4 pixels (0.12 mm) were removed from the result. This algorithm was not used for quantitative analysis, but rather to observe relationships between increased MI and the retinal structure seen in the B-scans (Figs. 6, 7).

RESULTS

There were 24 eyes from 24 patients enrolled. The mean GA square root area at baseline was 2.0 mm (SD, 0.78), and after 1 year, the annual growth rate of GA in these study eyes was 0.4

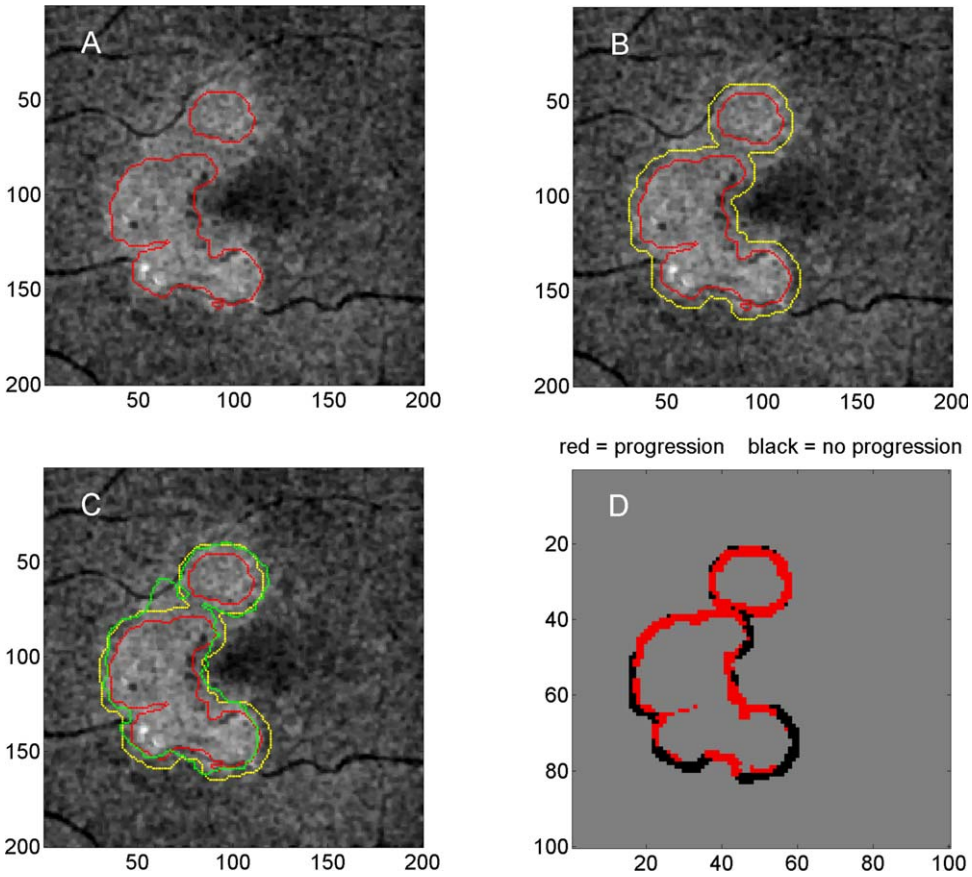

FIGURE 4. Extraction of MI values from areas of progression and nonprogression at the edge of GA. (**A**) MI image from the initial baseline scan, with the area of GA at baseline outlined in *red*. The GA segmentation was obtained from the baseline scan sub-RPE slab. (**B**) The *yellow line* depicts the 180-μm perimeter around the baseline perimeter of the GA segmentation (*red*). The *red* and *yellow* contours enclose the area to be analyzed. (**C**) The area of GA at 52-week follow-up is outlined in *green*. The segmentation of the 52-week sub-RPE slab was registered to the position of the initial baseline scan. (**D**) Areas of 52-week progression (*red*) and nonprogression (*black*) are found within the 180-μm perimeter of the baseline GA segmentation. Pixels are downsampled by 2 in each direction to eliminate statistical dependence due to smoothing of adjacent pixels.

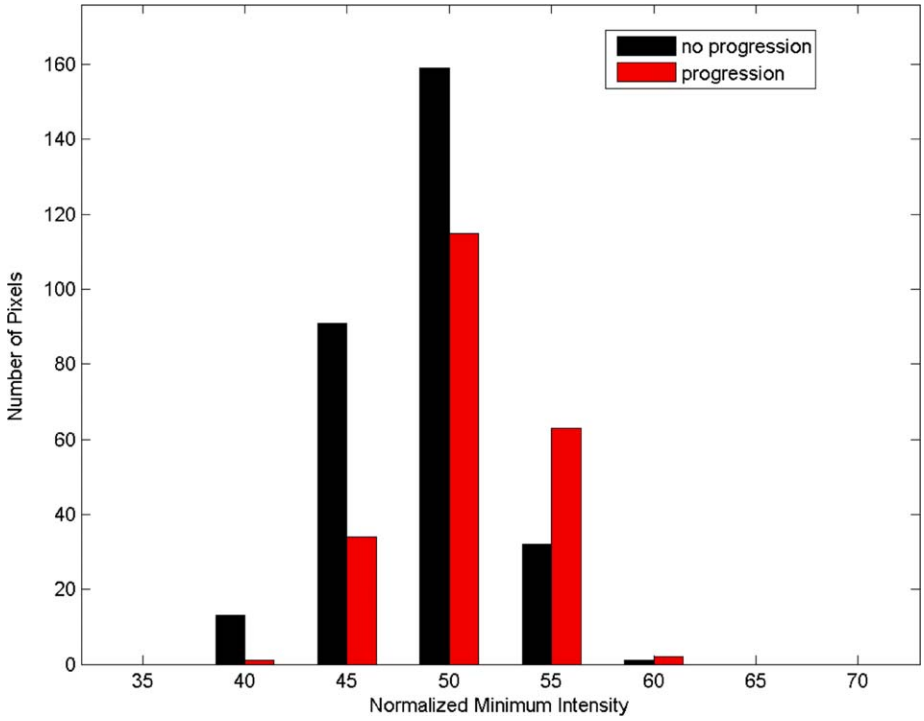

Figure 5. Histogram of normalized baseline MIs within 180 μm of edge of GA from baseline scan for a typical case. While there is a large overlap between the MIs of the areas within the 180-μm border region that later progressed to GA and of those that did not, on the whole there was significant increase ($P < 0.01$) for this eye in areas that later progressed to GA.

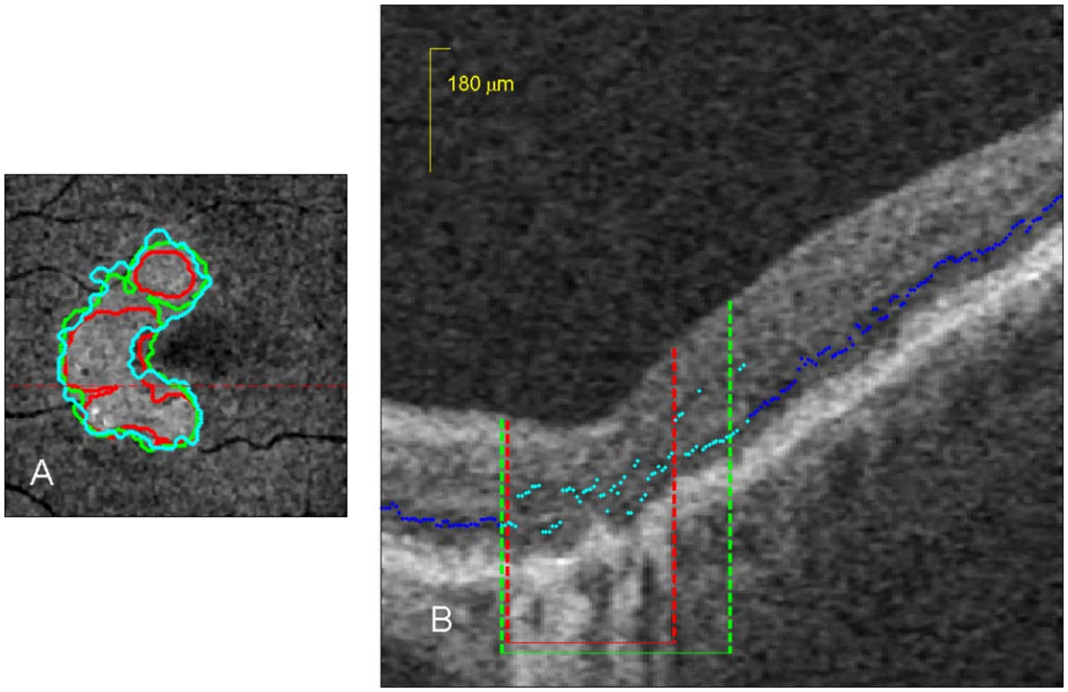

Figure 6. Example of an en face MI image from baseline OCT scan, with selected B-scan showing locations of minima, area of increased MI at baseline, area of GA at baseline, and area of GA at 52-week follow-up. (**A**) En face OCT MI image. *Red* outline indicates GA segmentation determined using sub-RPE slab from this same OCT data volume. *Green* outline indicates GA segmentation determined using sub-RPE slab from 52-week follow-up OCT scan, registered into coordinates of the scan shown here. *Light blue* outline indicates region of increased MI determined by thresholding the MI image. *Red dashed line* indicates location of selected B-scan. (**B**) Speckle-reduced B-scan, zoomed vertically. Points of increased MI (determined by thresholding the en-face MI image) in *light blue*; points of normal MI in *dark blue. Red bracket* indicates the GA segmentation determined using sub-RPE slab from this same OCT data volume. *Green bracket* indicates the registered GA segmentation from the 52-week follow-up scan. In this example, the region of increased MI includes the region of 52-week progression and slightly beyond. In this B-scan, all minima that occur above the ONL and HFL, indicating disruption of those layers, are contained within the region of increased MI.

Investigative Ophthalmology & Visual Science

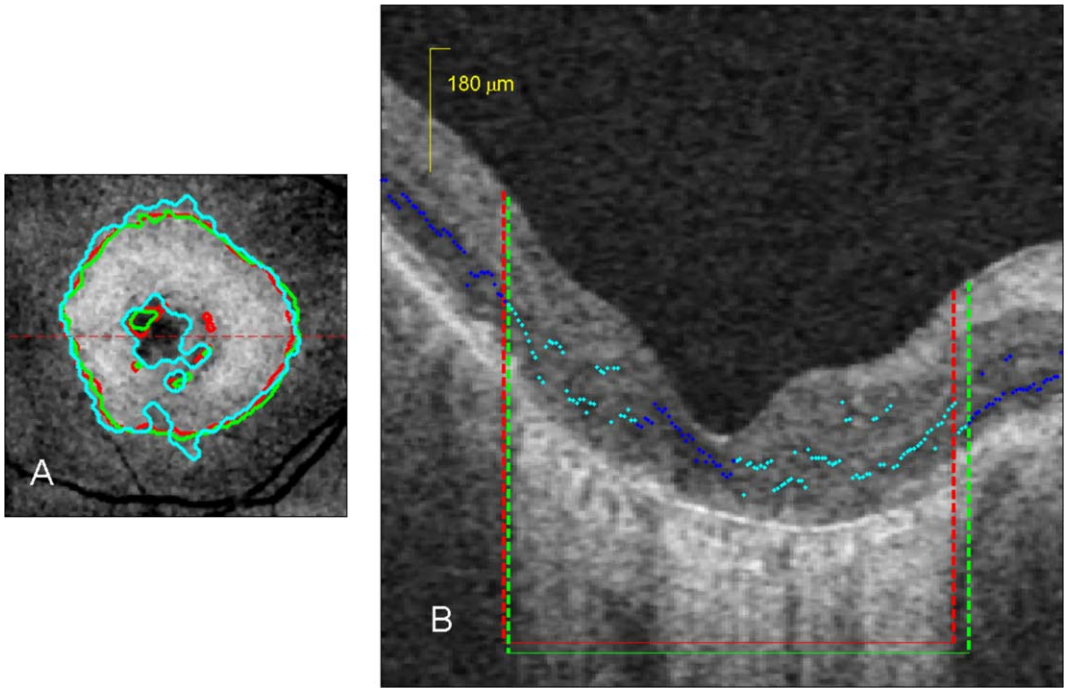

Figure 7. En face MI image from baseline OCT scan, with selected B-scan. (**A**) En face OCT MI image, showing that the MI at the fovea is lower than that of the surrounding area of GA. See Figure 6 for descriptions of color coding. (**B**) Speckle-reduced B-scan, zoomed vertically.

mm/y (SD, 0.24). All the scans at the 52-week follow-up could be well-registered to the baseline scans, so no scans needed to be excluded.

Nearly every case showed a statistically significant difference between the MI seen in areas of future progression and the MI in areas that did not progress. The MI was significantly higher ($P < 0.05$) in areas of growth in 21/24 cases (88%), and when the foveal subfield was excluded, in 22/24 cases (92%).

Although statistically different mean values were seen for areas of progression and nonprogression, there still was substantial overlap in the intensity distributions in these areas. This overlap was evident in the ROC analysis for predicting progression at specific locations, shown in Figure 8, as a low sensitivity and specificity of 61%. Figure 8 also shows that excluding the fovea had little effect on the ability to predict growth at specific locations.

When the fovea was included in the analysis, correlation of MI values with overall growth rate (Fig. 9) was not significantly greater than zero ($\rho = 0.35$, $P > 0.05$). When excluding the fovea, though, MI values correlated significantly with overall growth rate ($\rho = 0.47$, $P < 0.05$). Subjects with a root-area growth rate above the average for our sample were identified

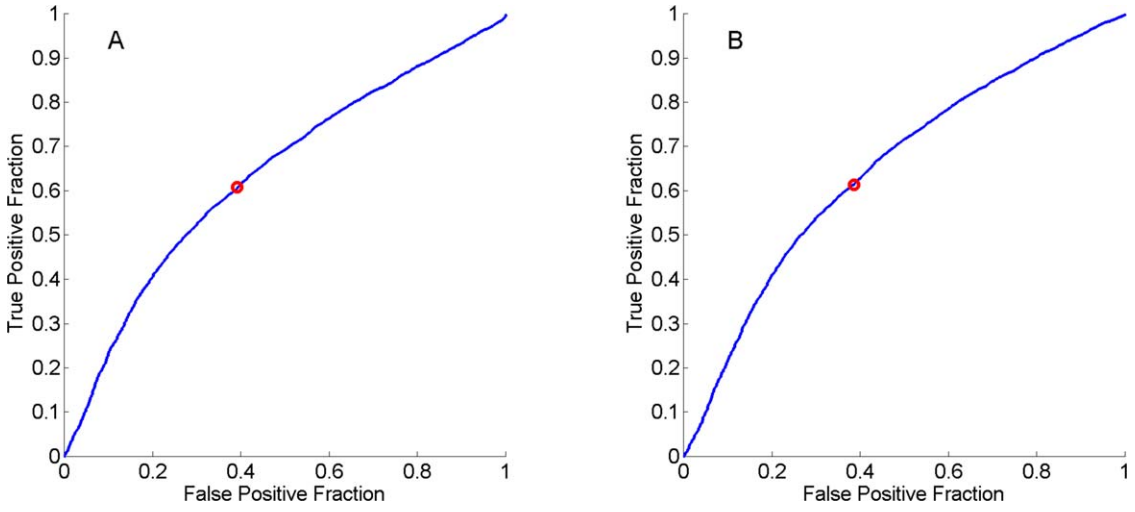

Figure 8. Analysis of sensitivity and specificity of the MI prediction of growth within the 180-μm border region at 52 weeks. The ROC curve plots true positive fraction (sensitivity) versus false positive fraction (1 − specificity) for the full range of possible threshold values. Here we plot the true positive and false positive fractions resulting from the range of thresholds on MI_{relative}, the average MI in the 180-μm margin measured relative to the average minimum intensities found in the lesion and background regions. (**A**) Using all data, including the fovea, a threshold value of 0.50 (indicated by *red circle*), predicted locations of growth with 61% sensitivity and 61% specificity. (**B**) Excluding the fovea from the analysis still gave 61% sensitivity and 61% specificity at a threshold value of 0.50.

Investigative Ophthalmology & Visual Science

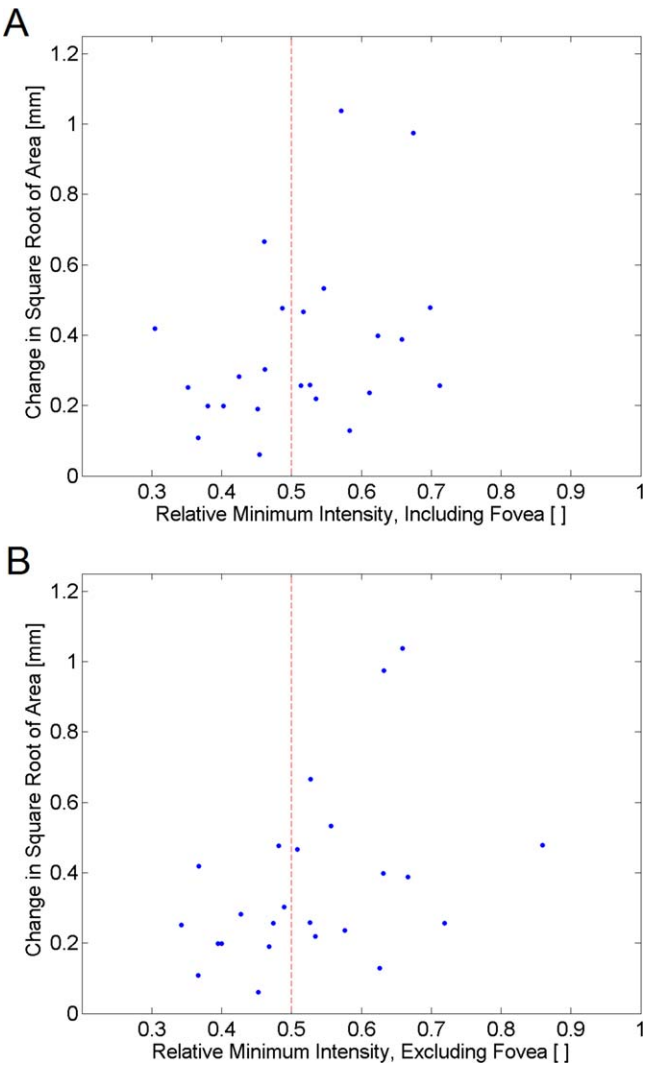

FIGURE 9. Scatterplots of overall growth rate versus relative MI ($MI_{relative}$) at the margin of GA. (**A**) Scatterplot including foveal data. (**B**) Scatterplot excluding foveal data.

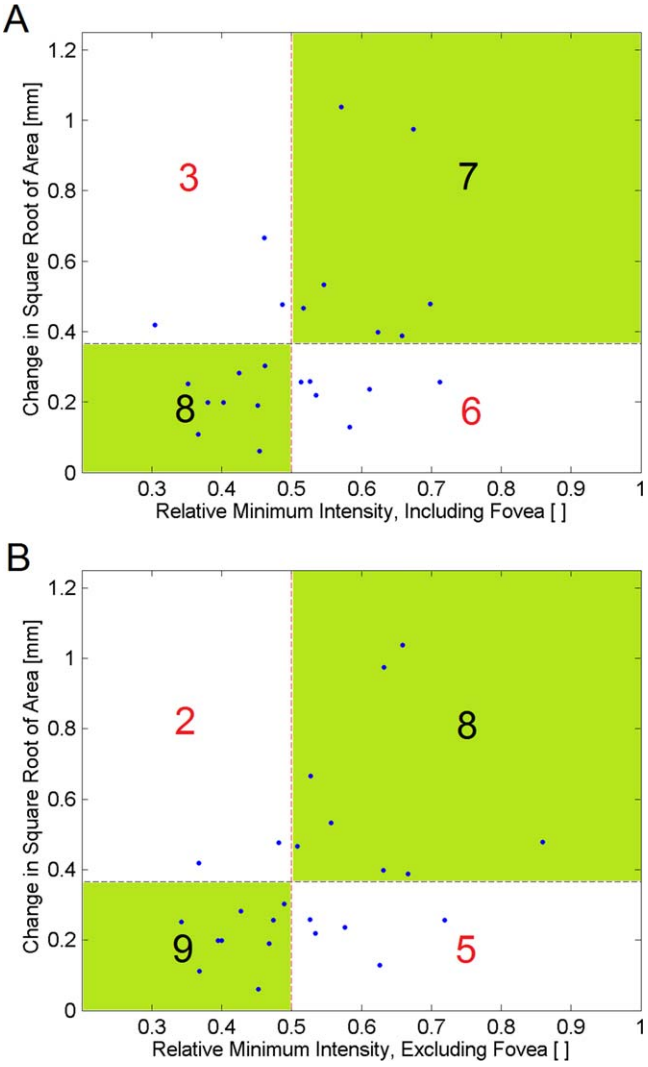

FIGURE 10. Scatterplots of overall growth rate versus relative MI ($MI_{relative}$) at the margin of GA for groups separated into above- and below-average growth rates. *Green* regions indicate areas of correct prediction, where $MI_{relative} > 0.5$ corresponded to an above-average growth rate or $MI_{relative} < 0.5$ corresponded to a below-average growth rate; *white* regions indicate areas of incorrect prediction. Large numbers indicate the number of subjects in each region. (**A**) Scatterplot including foveal data. (**B**) Scatterplot excluding foveal data.

with 70% sensitivity and 57% specificity when foveal regions were included in the analysis, but with 80% sensitivity and 64% specificity when the foveal regions were excluded (Fig. 10).

Review of B-scans (examples shown in Figs. 6, 7) demonstrated that increased MI typically corresponds with hyperreflectivity in the ONL/HFL, or atrophy of this layer, in which case the minimum is located in more reflective retinal layers.

Discussion

En face visualization of the minimum OCT intensities surrounding GA showed that an increased MI extended for varying distances beyond the margins of GA. Since the photoreceptor ONL and HFL have the lowest reflectivity in the normal retina for the wavelengths of light used in OCT, an increase in the MI would suggest that disruptions within those layers extend beyond the margins of the GA lesions. Although the ONL and HFL appear disrupted, inspection of the OCT B-scans showed that these layers still are present in these areas at the margin of the GA.

Since the MI generally is found within the ONL/HFL in areas of normal retina, an increase in MI is equivalent to an increase in the intensity of the ONL and HFL. In those areas of increased MI, identifying the layer where the minimum is located is not necessary simply to know that the ONL/HFL is exhibiting an abnormally elevated reflectivity. This elevated reflectivity presumably is due to some disruption of the photoreceptors at that location.

The GA had a slight tendency to grow into areas of increased MI rather than grow uniformly around the border of the GA. For approximately 90% of the subjects studied, the MI was significantly higher in areas of progression than it was in areas of nonprogression. Because the difference was small compared to the variation in MI within each type of region, though, there was a low sensitivity and specificity of prediction of localized areas of lesion growth.

A different behavior of the MI often was observed near the fovea, where the layers of the outer retina are thicker than they

are elsewhere (Fig. 7). Even inside a lesion of GA, the MI of the overlying tissue often was darker than that of the surrounding tissue. It is not known whether this is related to the progression of the GA. To separate this effect from the observations of the surrounding retina, analyses were performed with and without the data within 500 μm of the foveal center. This did not, however, affect the sensitivity and specificity of the prediction of locations of lesion growth.

Although it has been observed that photoreceptor loss occurs frequently outside the border of GA, the enlargement of GA as observed from OCT B-scans can vary greatly even at different points along the margin of the same lesion.[7] While an increase in MI appears to be associated with progression of GA, the weakness of the prediction at specific points may be related to the varied nature of the structural changes seen at the margin of GA. Although there appears to be a general tendency for photoreceptor disruption as depicted by MI to precede the appearance of GA, and to do so in nearly all patients, this does not appear to be uniformly true at all points along the margin of a lesion. Because of the varied nature of GA progression, even within a single lesion, a single metric may be unlikely to provide a comprehensive indicator of progression. The approach described here might be best used in conjunction with other characteristics, such as autofluorescence patterns, lesion topology, analysis of the deformation of the retinal layers, or another analysis of OCT reflectivity.

Another question addressed here is whether OCT can be used to identify patients who demonstrate rapid progression of GA. When the foveal subfield was excluded from the analysis of data at the margin, the subjects with above-average growth rates were identified with good sensitivity and low specificity. A generally increased MI at the margin of the GA could be a possible sign of overall disruption of the photoreceptors. This technique could be applied to the stratification of patient populations for drug studies.

Potential sources of error in this study included registration errors and segmentation errors. The registration of the baseline and follow-up scans was critical to determining the areas of progression and nonprogression of GA at the margin of the baseline segmentation. Due to patient motion during the scan, there may be abrupt shifts between adjacent B-scans that would prevent perfect registration. The registrations were checked manually to ensure that all the visible retinal landmarks were aligned within 100 μm. If the motion is assumed to be random then no consistent bias should be introduced by the possible presence of small errors, although the uncertainty in position could decrease the sensitivity and specificity of prediction of progression at specific locations. In addition to registration errors, some variability was introduced by possible inconsistencies in the manual segmentation due to image variability and the independent segmentation decisions for the baseline and follow-up scans. We expect that these errors would occur in both directions and that the net effect of these errors did not introduce a consistent bias. If the segmentations had tended to be consistently more conservative at one of the time points and more generous at the other, this could have a biasing effect; however, in our previous study (Stetson PF, et al. *IOVS* 2012;53:ARVO E-Abstract 2047), the same results also were seen whether the currently used baseline or the 13-week time point was used as a baseline. Since any biases in the initial baseline would have had a reversed effect on the results using the 13-week baseline, this ensures that the initial baseline did not contain biases large enough to affect the results. Since our results at 52 weeks compared to that initial baseline were consistent with the findings at 13 weeks compared to that initial baseline, we also can infer that the 52-week segmentations did not exhibit significant biases.

While this study did provide evidence to suggest that disruption of the ONL/HFL can predict the growth and progression of GA, the size of this study is small and additional patients are needed to determine the potential of this method for patient screening. Other future studies may look at the possibility of predicting the emergence of new lesions outside the margin of current lesions, whether the occurrence of decreased MI at the fovea also is related to GA progression, whether the relative depth of the minimum may have predictive power, and a comparison of patterns of GA with patterns of increased MI in healthier fellow eyes. Since the data in this study were limited to GA lesions contained within a 6×6 mm area around the fovea, it has not been determined whether the area of elevated MI continues to enlarge as the GA grows or if there is a limit to the area of the hyperreflectivity.

These findings suggested that there is an increase in MI at the margins of GA before enlargement and that this increase is located preferentially in the areas where the growth took place. This may indicate disruption or atrophy of the ONL and HFL in these areas before GA becomes apparent. This new en face imaging strategy suggests that the margin of GA where the photoreceptor cell bodies are disrupted may be more likely to progress to GA within one year of the time of imaging. Furthermore, it shows potential as a sensitive method for predicting the global severity of progression in individual patients. As an objective indicator of photoreceptor cell reflectivity changes, MI may prove useful as a predictor of enlargement and may be a useful parameter to monitor in eyes with dry AMD undergoing experimental therapies.

Acknowledgments

Supported by Alexion Phamaceuticals, Macula Vision Research Foundation, National Institutes of Health (NIH) Center Core Grant P30EY014801, Research to Prevent Blindness, Department of Defense (W81XWH-09-1-0675), and a grant from Carl Zeiss Meditec, Inc.

Disclosure: **P.F. Stetson**, Carl Zeiss Meditec, Inc. (I, E), P; **Z. Yehoshua**, None; **C.A.A. Garcia Filho**, None; **R. Portella Nunes**, Carl Zeiss Meditec, Inc. (F); **G. Gregori**, Carl Zeiss Meditec, Inc. (F); **P.J. Rosenfeld**, Acucela (C), Advanced Cell Technology (F), Alexion Pharmaceuticals (F), Bayer Healthcare Pharmaceuticals (C), Boehringer Ingelheim (C), Chengdu Kanghong Biotech (C), GlaxoSmithKline (F) Oraya (C), Sanofi/Genzyme (C), ThromboGenics (C), Carl Zeiss Meditec, Inc. (F)

References

1. Sunness JS, Gonzalez-Baron J, Applegate CA, et al. Enlargement of atrophy and visual acuity loss in the geographic atrophy form of age-related macular degeneration. *Ophthalmology*. 1999;106:1768–1779.
2. Sunness JS, Margalit E, Srikumaran D, et al. The long-term natural history of geographic atrophy from age-related macular degeneration: enlargement of atrophy and implications for interventional clinical trials. *Ophthalmology*. 2007;114:271–277.
3. Yehoshua Z, Rosenfeld PJ, Gregori G, et al. Progression of geographic atrophy in age related macular degeneration imaged with spectral domain optical coherence tomography. *Ophthalmology*. 2011;118:679–686.
4. Lujan BJ, Rosenfeld PJ, Gregori G, et al. Spectral domain optical coherence tomographic imaging of geographic atrophy. *Ophthalmic Surg Lasers Imaging*. 2008;39(suppl 4):S8–S14.
5. Helb HM, Charbel Issa P, Fleckenstein M, et al. Clinical evaluation of simultaneous confocal scanning laser ophthalmoscopy imaging combined with high-resolution, spectral-domain optical coherence tomography. *Acta Ophthalmol*. 2010;88:842–849.

6. Fleckenstein M, Schmitz-Valckenberg S, Martens C, et al. Fundus autofluorescence and spectral-domain optical coherence tomography characteristics in a rapidly progressing form of geographic atrophy. *Invest Ophthalmol Vis Sci*. 2011;52:3761–3766.
7. Bearelly S, Chau FY, Koreishi A, Stinnett SS, Izatt JA, Toth CA. Spectral domain optical coherence tomography imaging of geographic atrophy margins. *Ophthalmology*. 2009;116:1762–1769.
8. Fleckenstein M, Charbel Issa P, Helb HM, et al. High-resolution spectral domain-OCT imaging in geographic atrophy associated with age-related macular degeneration. *Invest Ophthalmol Vis Sci*. 2008;49:4137–4144.
9. Fleckenstein M, Schmitz-Valckenberg S, Adrion C, et al. Tracking progression with spectral-domain optical coherence tomography in geographic atrophy caused by age-related macular degeneration. *Invest Ophthalmol Vis Sci*. 2010;51:3846–3852.
10. Schmitz-Valckenberg S, Fleckenstein M, Gobel AP, Hohman TC, Holz FG. Optical coherence tomography and autofluorescence findings in areas with geographic atrophy due to age-related macular degeneration. *Invest Ophthalmol Vis Sci*. 2011;52:1–6.
11. Sayegh RG, Simader C, Scheschy U, et al. A systematic comparison of spectral-domain optical coherence tomography and fundus autofluorescence in patients with geographic atrophy. *Ophthalmology*. 2011;118:1844–1851.
12. Jiao S, Knighton RW, Huang X, et al. Simultaneous acquisition of sectional and fundus ophthalmic images with spectral-domain optical coherence tomography. *Opt Express*. 2005;13:444–452.
13. Wojtkowski M, Srinivasan V, Fujimoto JG, et al. Three-dimensional retinal imaging with high-speed ultrahigh-resolution optical coherence tomography. *Ophthalmology*. 2005;112:1734–1746.
14. Yehoshua Z, Garcia Filho CA, Penha FM, et al. Comparison of geographic atrophy measurements from the OCT fundus image and the sub-RPE slab image. *Ophthalmic Surg Lasers Imaging Retina*. 2013;44:127–132.
15. Lindblad AS, Lloyd PC, Clemons TE, et al. Change in area of geographic atrophy in the Age-Related Eye Disease Study: AREDS report number 26. *Arch Ophthalmol*. 2009;127:1168–1174.
16. Holz FG, Bindewald-Wittich A, Fleckenstein M, Dreyhaupt J, Scholl HP, Schmitz-Valckenberg S. Progression of geographic atrophy and impact of fundus autofluorescence patterns in age-related macular degeneration. *Am J Ophthalmol*. 2007;143:463–472.
17. Bhutto I, Lutty G. Understanding age-related macular degeneration (AMD): relationships between the photoreceptor/retinal pigment epithelium/Bruch's membrane/choriocapillaris complex. *Mol Aspects Med*. 2012;33:295–317.
18. Pumariega NM, Smith RT, Sohrab MA, Letien V, Souied EH. A prospective study of reticular macular disease. *Ophthalmology*. 2011;118:1619–1625.
19. Zweifel SA, Imamura Y, Spaide TC, Fujiwara T, Spaide RF. Prevalence and significance of subretinal drusenoid deposits (reticular pseudodrusen) in age-related macular degeneration. *Ophthalmology*. 2010;117:1775–1781.
20. Davis MD, Gangnon RE, Lee LY, et al. The Age-Related Eye Disease Study severity scale for age-related macular degeneration: AREDS Report No. 17. *Arch Ophthalmol*. 2005;123:1484–1498.
21. Ferris FL, Davis MD, Clemons TE, et al. A simplified severity scale for age-related macular degeneration: AREDS Report No. 18. *Arch Ophthalmol*. 2005;123:1570–1574.
22. Schmitz-Valckenberg S, Alten F, Steinberg JS, et al. Reticular drusen associated with geographic atrophy in age-related macular degeneration. *Invest Ophthalmol Vis Sci*. 2011;52:5009–5015.
23. Schmitz-Valckenberg S, Bindewald-Wittich A, Dolar-Szczasny J, et al. Correlation between the area of increased autofluorescence surrounding geographic atrophy and disease progression in patients with AMD. *Invest Ophthalmol Vis Sci*. 2006;47:2648–2654.
24. Schmitz-Valckenberg S, Fleckenstein M, Scholl HP, Holz FG. Fundus autofluorescence and progression of age-related macular degeneration. *Surv Ophthalmol*. 2009;54:96–117.
25. Brar M, Kozak I, Cheng L, et al. Correlation between spectral-domain optical coherence tomography and fundus autofluorescence at the margins of geographic atrophy. *Am J Ophthalmol*. 2009;148:439–444.
26. Parisi V, Perillo L, Tedeschi M, et al. Macular function in eyes with early age-related macular degeneration with or without contralateral late age-related macular degeneration. *Retina*. 2007;27:879–890.
27. Sunness JS, Johnson MA, Massof RW, Marcus S. Retinal sensitivity over drusen and nondrusen areas. A study using fundus perimetry. *Arch Ophthalmol*. 1988;106:1081–1084.
28. Sunness JS, Schuchard RA, Shen N, Rubin GS, Dagnelie G, Haselwood DM. Landmark-driven fundus perimetry using the scanning laser ophthalmoscope. *Invest Ophthalmol Vis Sci*. 1995;36:1863–1874.
29. Meleth AD, Mettu P, Agron E, et al. Changes in retinal sensitivity in geographic atrophy progression as measured by microperimetry. *Invest Ophthalmol Vis Sci*. 2011;52:1119–1126.
30. Midena E, Vujosevic S, Convento E, Manfre A, Cavarzeran F, Pilotto E. Microperimetry and fundus autofluorescence in patients with early age-related macular degeneration. *Br J Ophthalmol*. 2007;91:1499–1503.
31. Phipps JA, Dang TM, Vingrys AJ, Guymer RH. Flicker perimetry losses in age-related macular degeneration. *Invest Ophthalmol Vis Sci*. 2004;45:3355–3360.
32. Luu CD, Dimitrov PN, Robman L, et al. Role of flicker perimetry in predicting onset of late-stage age-related macular degeneration. *Arch Ophthalmol*. 2012;130:690–699.
33. Sunness JS, Rubin GS, Broman A, Applegate CA, Bressler NM, Hawkins BS. Low luminance visual dysfunction as a predictor of subsequent visual acuity loss from geographic atrophy in age-related macular degeneration. *Ophthalmology*. 2008;115:1480–1488.
34. Nunes RP, Gregori G, Yehoshua Z, et al. Predicting the progression of geographic atrophy in age-related macular degeneration with sd-oct en face imaging of the outer retina. *Ophthalmic Surg Lasers Imaging Retina*. 2013;44:344–359.
35. Stetson PF. Non-linear projections of 3-D medical imaging data. US Patent 8,332,016, December 11, 2012.
36. Neri E, Bartolozzi C. *Image Processing in Radiology: Current Applications*. Berlin, Germany: Springer Verlag; 2008.
37. Bankman IN. *Handbook of Medical Image Processing and Analysis*. Burlington, MA: Elsevier Academic Press; 2009.
38. Napel S, Rubin GD, Jeffrey RB Jr. STS-MIP: a new reconstruction technique for CT of the chest. *J Comput Assist Tomogr Sep-Oct*. 1993;17:832–838.
39. Stetson PF, Bagherinia H. Method for finding the lateral position of the fovea in an SDOCT image volume. US Patent 8,079,711, December 20, 2011.
40. Stetson PF, Bagherinia H. Method for finding the lateral position of the fovea in an SDOCT image volume. US Patent 8,251,511, August 28, 2012.

Investigative Ophthalmology & Visual Science